Available online at www.sciencedirect.com
ScienceDirect
C. R. Physique 10 (2009) 188–196
COMPTES RENDUS PHYSIQUE

Laser acceleration of particles in plasmas / Accélération laser de particules dans les plasmas

Dynamic control and enhancement of laser-accelerated protons using multiple laser pulses

David C. Carroll [a], Dimitri Batani [g], Roger G. Evans [d], Yannick Glinec [c], Christian Homann [c], Rashida Jafer [g], Satyabrata Kar [e], Filip Lindau [c], Olle Lundh [c], Keith Markey [e], David Neely [b], Frank Nürnberg [f], Anders Persson [c], Mark N. Quinn [a], Alex P.L. Robinson [b], Markus Roth [f], Claes-Göran Wahlström [c], Xiaohui Yuan [a], Matthew Zepf [e], Paul McKenna [a,*]

[a] *SUPA, Department of Physics, University of Strathclyde, Glasgow, G4 0NG, UK*
[b] *STFC, Rutherford Appleton Laboratory, Didcot OX11 0QX, UK*
[c] *Department of Physics, Lund University, P.O. Box 118, 221 00 Lund, Sweden*
[d] *The Blackett Laboratory, Imperial College London, London, SW7 2AZ, UK*
[e] *School of Mathematics and Physics, Queens University Belfast, Belfast BT7 1NN, UK*
[f] *Technische Universität Darmstadt, Institut für Kernphysik, Schlossgartenstr. 9, 64289 Darmstadt, Germany*
[g] *Dipartimento di Fisica, Università di Milano Bicocca, 20126 Milano, Italy*

Available online 28 April 2009

Abstract

The use of schemes involving multiple laser pulses to enhance and control the properties of beams of protons accelerated in ultra-intense laser irradiation of planar foil targets is discussed. Specifically, the schemes include the use of a second laser pulse to produce and control preplasma expansion of the target to enhance energy coupling to the proton beam; the use of a second laser pulse to drive shock deformation of the target to change the direction of the proton beam; and a scheme involving dual high intensity laser pulses to change the properties of the sheath field, with the aim of modifying the proton energy spectrum. An overview of our recent experimental and theoretical results is given. The overall aim of this work is to determine the extent to which the properties of the sheath-accelerated proton beam can be optically controlled, to enable beam delivery at high repetition rates. ***To cite this article: D.C. Carroll et al., C. R. Physique 10 (2009).***

Résumé

Contrôle dynamique et enrichissement d'un faisceau de protons, accéléré par laser, en utilisant des impulsions multiples. Le recours à des régimes utilisant plusieurs impulsions laser afin d'améliorer et de contrôler les caractéristiques des faisceaux de protons accélérés par l'interaction d'une impulsion laser ultra intense avec une cible solide est discuté. Plus particulièrement, l'utilisation d'une seconde impulsion laser pour produire un pré-plasma et en contrôler l'expansion afin d'augmenter le couplage entre l'énergie du laser et celle du faisceau de protons, ainsi que l'utilisation d'une seconde impulsion laser pour induire une déformation par choc de la cible afin de changer la direction du faisceau de protons sont discutés. Un régime impliquant l'utilisation de deux impulsions laser à haute intensité pour changer les propriétés du champ accélérateur dans le but de modifier la distribution

* Corresponding author.
E-mail address: p.mckenna@phys.strath.ac.uk (P. McKenna).

1631-0705/$ – see front matter
doi:10.1016/j.crhy.2009.03.003

énergétique des protons sont également discuté. Nos derniers résultats expérimentaux et théoriques sont présentés. Ces travaux ont été réalisés afin de déterminer jusqu'où il est possible de contrôler les propriétés des faisceaux d'ions accélérés par interaction laser–plasma en s'appuyant sur des méthodes optiques, ceci afin de pouvoir fournir ces faisceaux à un taux de répétition élevée.
Pour citer cet article : D.C. Carroll et al., C. R. Physique 10 (2009).

Keywords: Laser–particle acceleration; Proton beam; Laser–plasma interactions

Mots-clés : Accélération laser de particules ; Faisceau de protons ; Interactions laser–plasma

1. Introduction

Multi-MeV ion acceleration driven by ultrashort, high power laser pulse interactions with thin metallic foil targets continues to attract considerable interest, due to the unique properties of the ion beam (short pulse, high brightness and ultralow emittance) and the compact nature of the source [1]. At the laser intensities presently available, the predominant ion acceleration mechanism is Target Normal Sheath Acceleration (TNSA) [2], which occurs at the rear of the target and is driven by fast electrons transported through the target from the laser-irradiated front surface. Due to it's high charge-to-mass ratio and the presence of hydrogenated contamination layers on the target surfaces, the proton is the most efficiently accelerated ion species.

Many potential applications of laser-accelerated proton beams have been proposed, including ion radiotherapy [3–5], isotope production for medical imaging techniques [6,7], nuclear activation studies [8,9], injectors for the next generation of ion accelerators [10,11] and laser-ion driven fast ignition [12,13]. The successful realisation of many of these applications requires the development of techniques to enhance and control the source and beam properties. One method to achieve this involves the use of specialised targets. Using multi-layered targets, 'dot' targets and microdroplet targets, changes to the proton energy spectra have been demonstrated, including the production of a quasi-monoenergetic spectrum [14–16]. Curved targets and separate cylindrical targets have been used to demonstrate proton beam focusing [17,18] and defocusing [19], targets with a cylindrical ('washer') structure attached to the rear surface have been used to change the beam divergence [20] and targets with micro- and nano-structured front surfaces have been used to enhance energy coupling to protons [21]. However, the reliance on complex or specialised targets is not always compatible with the requirement of high repetition rate ion beam delivery for many applications. Dynamic control of the beam properties, using optical techniques involving one or more laser pulses (operating at high repetition rate) and simple planar target foils is desirable.

In this article we discuss several schemes incorporating the use of a second laser pulse to enhance and control properties of the beam of protons accelerated by an ultrahigh intensity laser pulse. We begin with a report on a first experiment into the effects of controlled and well-characterised plasma expansion on the energy, flux and uniformity of beams of accelerated protons. The plasma expansion is controlled using a low intensity pulse synchronised to the main proton acceleration driver pulse. A scheme involving a similar beam arrangement to induce dynamic control of the curvature of the target using laser-driven shock waves is presented next. Finally the use of dual high intensity pulses to control the proton energy spectrum is discussed.

2. Enhancing beam energy, flux and uniformity

During the interaction of a high power laser pulse with a thin foil target, prepulses or Amplified Spontaneous Emission (ASE) at the leading edge of the pulse typically produces plasma expansion at the front, irradiated surface of the target. Even if the target rear surface is unperturbed by the preheating, the properties of the ion beam produced at the rear surface are affected by the change to the laser energy absorption and fast electron generation at the front surface. Recent theoretical studies have shown that laser absorption efficiency (and therefore proton acceleration) can be enhanced by controlling the scale length of the front surface preplasma [22,23]. This effect has also been experimentally observed at laser intensities of between 10^{18} and 10^{19} $\mathrm{W\,cm^{-2}}$ using ultrashort (tens of femtosecond) laser pulses [24,25]. In these experiments, changes to the preplasma expansion was produced by changing the intensity contrast (ratio of the peak laser intensity to the intensity of the ASE). We recently performed a controlled and well-characterised experiment using the Vulcan laser at the Rutherford Appleton Laboratory to investigate to what

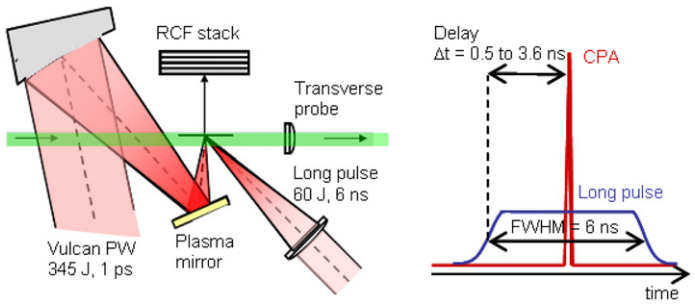

Fig. 1. (a) Schematic of the experiment showing the laser beam arrangement and primary diagnostics: RCF stack and transverse interferometric probe. (b) The relative temporal position of the low intensity ablation pulse ('long pulse') and the main CPA beam.

extent preplasma expansion, controlled using a separate synchronised laser pulse, can be used to enhance laser energy coupling to protons, in the ultraintense (3×10^{20} W cm^{-2}) picosecond laser pulse regime [26,27].

The details of the experiment are described elsewhere [27], and the arrangement is shown in Fig. 1. In brief, we use two beams from the Vulcan laser, one to produce controlled preplasma expansion and one to drive proton acceleration. A third beam is used to characterise the plasma expansion. Proton acceleration is driven by the main Chirped Pulse Amplified (CPA) pulse with wavelength (λ) equal to 1054 nm and pulse duration equal to 1 ps (FWHM). The intensity contrast of this beam is enhanced using a plasma mirror [28,29] to suppress the intensity of the ASE pedestal to $<10^{11}$ W cm^{-2}. The mirror has a measured reflectivity of 32%, resulting in a maximum on-target pulse energy equal to 115 J. The CPA pulses are incident on target at 10° and focused to a peak intensity, I_{CPA}, equal to 3×10^{20} W cm^{-2}. Plasma expansion is produced using low energy laser pulses of 6 ns duration (rise time equal to 0.2 ns) and wavelength equal to 1054 nm. The pulses are focused to an approximately flat-top intensity distribution, diameter equal to 450 μm, on the front surface of the target. The CPA beam is focused into the centre of this distribution. The preplasma expansion is varied by changing the intensity of the 'ablation pulse', I_{abl}, in the range 0.5 to 5 TW cm^{-2}, and the temporal separation of the two pulses, Δt, in the range 0.5 to 3.6 ns, with 0.2 ns precision. The plasma expansion is characterised using a frequency doubled (527 nm) interferometric probe beam. Interferograms of the plasma expansion are recorded 5 ps after the arrival of the CPA pulse and with a spatial resolution of 5 μm.

The targets are 25 μm-thick planar Cu or Au foils. The Au foils have a periodic groove structure (lines) on the rear surface to enable determination of the proton source size and beam emittance [30,31]. Passive stacks of dosimetry film (RCF, Gafchromic© HD-810 and MD-V2-55) are used to measure the spatial and energy distributions of the proton beam.

The plasma expansion is systematically changed in two ways: by varying I_{abl} for fixed $\Delta t = 0.5$ ns, and by varying Δt for fixed $I_{\mathrm{abl}} = 1$ TW cm^{-2}. The resulting electron density profiles at the target front surface are measured using the interferometric probe. Example results are shown in Fig. 2, for $\Delta t = 0.5$ ns and 3.6 ns. 2-D hydrodynamic simulations are performed for the parameters of the experiment, and the results included for comparison in Fig. 2. The details of the simulation, using the POLLUX code [32], are provided elsewhere [27]. Two distinct regions of preplasma expansion are clearly observed. Hereafter, we refer to the scale length of the underdense outer part of the preplasma as L_{O}, and we refer to the density scale length in the inner region, in the region of the critical density, as L_{I}. Experimental values of L_{O} are determined by fitting the equation $n_e(x) = n_0 \times \exp(-x/L_{\mathrm{O}})$, where $n_e(x)$ is the electron density as a function of distance from the target surface, to the density profile extracted from the interferometric probe measurements. Typically measured values of L_{O} range from 50 ± 10 μm to 200 ± 40 μm for an increase in Δt from 0.5 ns to 3.5 ns. For comparison, the simulation results predict increases in L_{O} from 31 μm to 182 μm and in L_{I} from ∼0.6 μm to ∼0.9 μm. An upper estimate of $L_{\mathrm{O}} = 5$ μm for the plasma expansion due to the ASE is measured from interferometric probe images.

It should be noted that the range of I_{abl} and Δt parameters experimentally investigated is limited by the requirement that the shock wave launched into the target by the ablation pressure at the front surface should not reach the rear surface of the targets before the arrival of the CPA pulse. The calculated position of the shock front, using the approach and parameters given in Lundh et al. [33], as a function of I_{abl} and for given Δt is shown in Fig. 2. The absence of target rear surface expansion is confirmed by the hydrodynamic simulation results and experimentally in the interferograms.

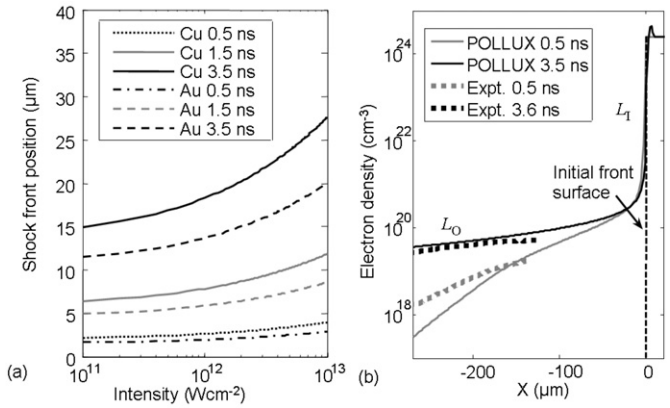

Fig. 2. (a) Calculated shock front positions in Cu and Au, as a function of I_{abl} at given Δt; (b) Density profile at the front surface of a Cu target as a function of expansion time, calculated using the POLLUX hydrodynamic code. The dashed line corresponds to the initial target surface. A dual exponential density profile is observed and is characterised with two density scale lengths. These correspond to an underdense, outer region (L_O) and an overdense, inner region (L_I). Corresponding experimental measurements of the electron density in the L_O region are also shown in (b).

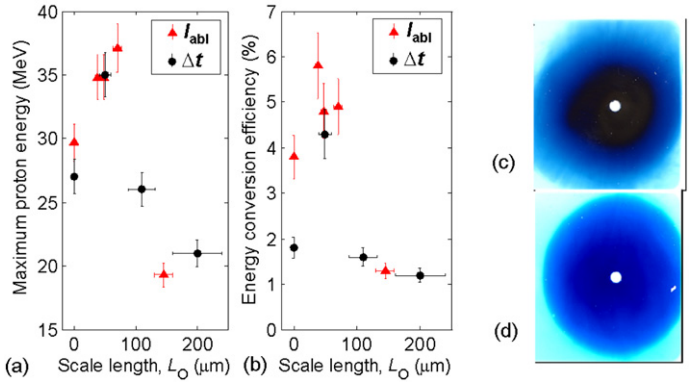

Fig. 3. (a) The measured maximum proton energy (E_{max}) as a function of experimentally measured L_O for the I_{abl} and Δt parameter scans. (b) The conversion efficiency (η) of laser energy into protons as a function of L_O. (c) and (d): Representative examples of the measured 9.5 MeV proton spatial intensity distributions for (c) no ablation pulse and (d) $I_{abl} = 5.0\ \mathrm{TW\,cm^{-2}}$.

Fig. 3 summarises some of the measured changes to the proton beam. As L_O is increased up to ∼60 μm, significant increases are measured in both the maximum proton energy, E_{max}, and the efficiency of conversion, η, of laser energy to protons. The conversion efficiency is the total proton beam energy for proton energies above 2 MeV as a percentage of the laser energy on target. These beam parameters are found to decrease again as L_O is increased up to ∼100 μm, to values smaller than achieved with a sharp density gradient (no ablation pulse). The same optimum scale length is observed by changing I_{abl} or Δt. Notable improvements are also observed in the spatial intensity profile of the proton beam, for all cases in which a preplasma expansion is produced. Example measurements are shown in Fig. 3. Improvements in both the beam uniformity and circularity, over the full proton energy range, are quantified and reported in Refs. [26,27].

From interferometric probe measurements made 5 ps after the CPA pulse, we determine that many of the measured changes to the proton beam parameters are likely to result from changes to the CPA pulse propagation in the expanding underdense plasma. This is discussed in Ref. [27]. For the conditions of optimum E_{max} and η there is evidence of channelling or self-focusing of the CPA beam, whereas the longer scale preplasma is shown to result in break up of the propagating CPA pulse, resulting in energy deposition over a larger area than the nominal focal spot size of the CPA laser [27]. The resulting changes to the laser intensity qualitatively explain the changes to the proton beam parameters.

To gain further insight into the effects of the preplasma expansion on the CPA absorption and electron acceleration near the critical density, we perform OSIRIS [34] particle-in-cell (PIC) simulations. A 40 μm by 20 μm grid with

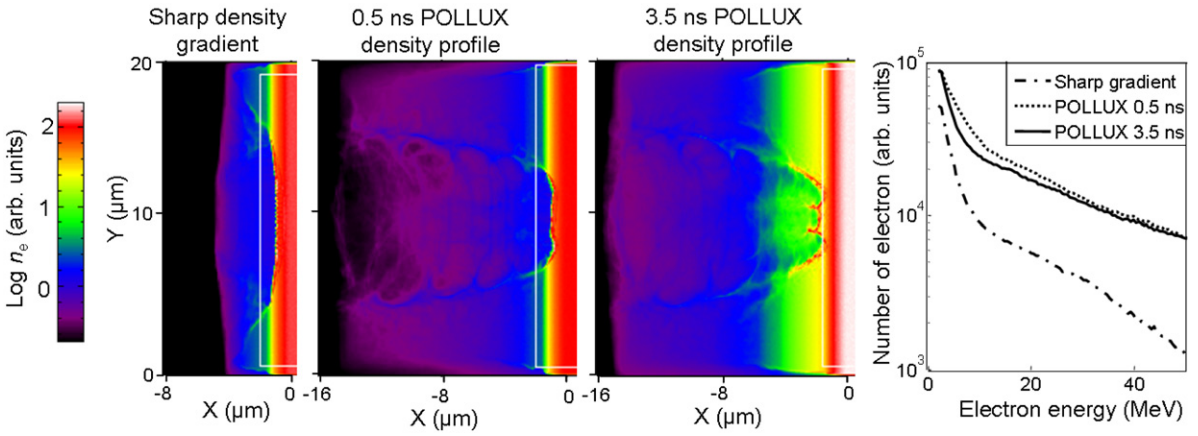

Fig. 4. Electron density, n_e, maps from 2D OSIRIS simulations as a function of the initial density profile (output from POLLUX). (a) The case of a sharp density gradient where there is little preplasma expansion. (b) and (c): The results for the initial electron density profiles provided by the POLLUX simulation for $\Delta t = 0.5$ ns and 3.5 ns, respectively. (d) Integrated electron energy distributions for the various initial n_e profiles. The sharp density gradient profile is two linear ramps: a density decrease from solid to 10× critical over 1 μm and from 10× critical to zero over 5 μm.

8000 by 4000 cells, and 4 electrons and 4 ions per cell, is used. The laser is linearly polarised with the E-vector in the simulation plane. The focal spot is 10 μm and pulse rise time is 15 fs, with measurements made 40 fs after the start of the pulse. The laser pulse duration is limited to 60 fs due to available computing resources. Three example results are shown in Fig. 4 for three different initial density profiles: the two density profiles calculated using POLLUX for $\Delta t = 0.5$ ns and 3.5 ns (Fig. 2) and a steeper density gradient. In qualitative agreement with our experimental observations, evidence of self-focusing is observed for $\Delta t = 0.5$ ns (compared to the steeper density gradient) and beam disruption is observed for $\Delta t = 3.5$ ns. A significant increase in electron flux is observed at all energies in the presence of preplasma expansion, but little difference is observed for the two cases $\Delta t = 0.5$ ns and 3.5 ns.

The results from this investigation highlight that an optimal preplasma expansion exists for enhanced proton flux and energy, and that this can be controlled using a separate low intensity laser pulse. The findings also demonstrate the importance of understanding the effects of variable density scale length plasmas on the coupling of laser energy into fast electrons for applications such as the fast ignition scheme for fusion energy.

3. Control of beam direction and divergence

Ions accelerated by the TNSA mechanism are directed along the localised target normal at the rear surface of the target. It has been shown that a low temperature shock wave launched into the target can, upon reaching the rear surface, deform the rear surface and alter the direction of proton acceleration [33,35,36]. The use of a separate low intensity laser pulse to control the spatial and temporal properties of the low temperature shock, and thereby control the direction of the proton beam, is reported by Lundh et al. [37] and discussed here.

The investigation is conducted at the Lund Laser Centre using the multi-Terawatt laser system. The main CPA laser beam is focused onto target to a spot size of 5 μm (FWHM) giving a peak intensity of $\sim 4 \times 10^{19}$ W cm^{-2} (600 mJ in 45 fs (FWHM)). A 3 μm thick planar Al foil target is irradiated by the p-polarised main laser pulse at a 30° incidence angle. Care is taken to ensure good laser pulse contrast [37] and is measured to be 10^{10} at 1 ns and 10^{9} at 50 ps before the main CPA pulse. A 11 ns low intensity ($\sim 3 \times 10^{10}$ W cm^{-2}) long pulse synchronised with the main CPA beam is used to drive a low temperature shock wave into the target. This pulse is focused with a tilted 200 mm focal length doublet lens to produce a horizontal line focus (230 μm long and 14 μm wide). The delay, Δt, between the half-maximum of the rising edge of the low intensity pulse and the peak of the main CPA pulse is controlled. Δt is varied from 3 to 12 ns with an error of 0.2 ns, while keeping all other laser parameters constant (relative line focus position of −15 μm). The position of the low intensity line focus, relative to the focal spot of the main CPA beam is varied from −30 μm (below CPA spot) to +30 μm (above CPA spot), whilst Δt is kept constant at 7.5 ns. The intensity of the ablation pulse I_{abl} (which drives the shock wave) is varied for $\Delta t = 7.5$ ns at −15 μm relative position. The spatial distribution of the proton beam is measured using CR39 covered by filter stripes of Al foil of varying thickness [35].

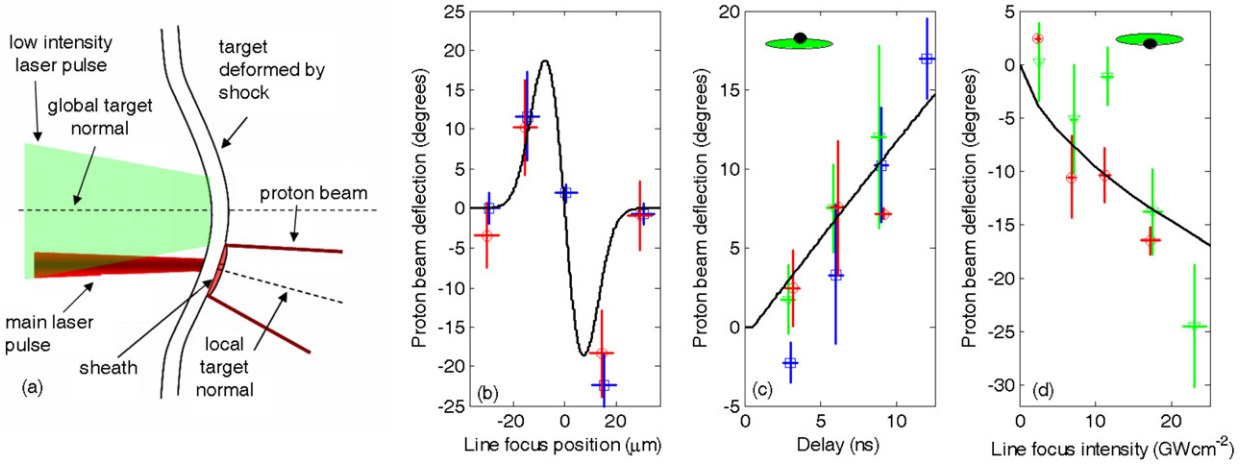

Fig. 5. (a) Illustration of proton beam steering by shock deformation of target. (b)–(d) Measured angular deflection of the proton beam as a function of: (b) the relative position of the line focus (fixed intensity of 2.5×10^{10} W cm^{-2} and $\Delta t = 7.5$ ns); (c) Δt (fixed intensity of 2.5×10^{10} W cm^{-2} and relative position of -15 μm); and (d) the intensity of the line focus (fixed $\Delta t = 7.5$ ns and relative position of $+10$ μm). The angular shift predicted by the rear surface shock deformation model reported in Ref. [37] is shown (black line). The relative position of the line and spot foci is shown schematically for (c) and (d). The proton energies are: blue squares 0.9 MeV, green triangles 1.4 MeV and red circles 2.8 MeV.

The low temperature shock, initiated by the low intensity pulse, propagates through the target and upon reaching the rear surface causes it to deform and expand outwards, as illustrated in Fig. 5(a), while retaining the steep density gradient required for ion acceleration. A shift of the entire proton beam implies that the rear surface deformation is large enough to encompass the entire accelerating sheath. The measured proton beam deflection as a function of Δt, I_{abl} and line focus position are shown in Fig. 5(b). Simple calculations of the shock transport and breakout using a quasi-two-dimensional scheme, described elsewhere [33,37], support the interpretation of shock-induced proton beam steering (Fig. 5(b)).

Optical steering of the proton beam accelerated from a thin target foil is demonstrated using low temperature shock waves produced by a separate low intensity laser pulse. The use of a separate shock driving laser enables the beam to be steered in any direction. A simple analytical model for shock deformation of the target rear surface is in good agreement with the experimental data. The results presented here demonstrate that an optically controlled shock can be used to manipulate the proton beam acceleration direction and offers the possibility that an annular ring induced shock wave could be used to induce a concave curvature of the target rear surface leading to dynamic control of proton beam focusing.

4. Spectral control

In addition to the beam characteristics discussed in the preceding sections, the actual energy spectrum of the beam is of critical importance to many applications. The vast majority of experiments have measured quasi-Maxwellian energy spectra, which are not suitable for certain applications. Some progress has been made in producing narrow-band energy spectra using carefully controlled target preparation [14,15]. Despite this, controlling the energy spectrum is still one of the biggest challenges in laser-driven ion acceleration.

Recently we proposed a radically different approach to the target engineering methods [38]. Independent research by Kumar and Pukhov [39] largely agrees with our findings. It was proposed that irradiating a foil target with two high intensity laser pulses in rapid succession could result in a modified energy spectrum that contained narrow peaks. This idea was studied using both one dimensional Vlasov simulations and PIC simulations. The full details of the numerical study are given in [38].

The scheme can be summarised as follows: The first laser pulse interacts with the foil and generates fast electrons with temperature T_1. These fast electrons drive proton acceleration at the rear surface of the foil. After a delay, a second pulse arrives and generates fast electrons with a higher temperature T_2. The sudden increase in the fast electron temperature does not merely provide a scalar enhancement to the electric field at the rear surface, it also

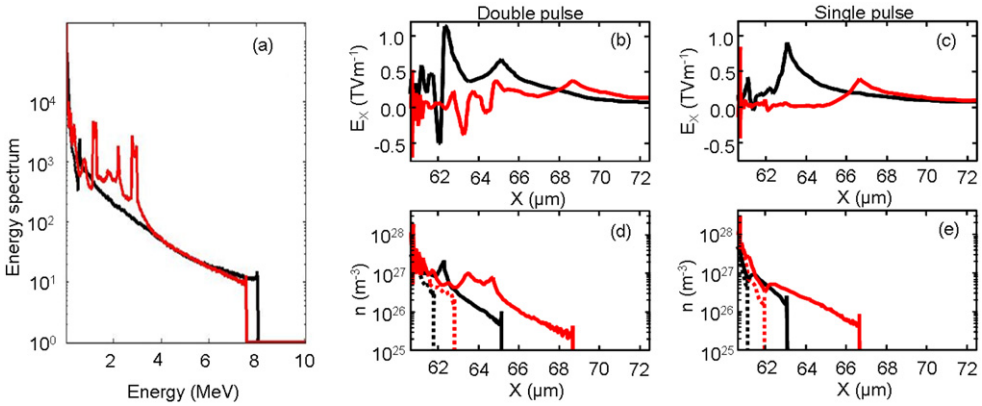

Fig. 6. (a) The proton spectra generated for single (black) and double (red) pulse regimes at 350 fs. (b) The electric field at the rear surface of the target at 240 fs (black) and 340 fs (red) for the double pulse regime. (c) The electric field at the rear surface of the target at 140 fs (black) and 240 fs (red) for the single pulse regime. The corresponding electron (solid line) and ion (dashed line) densities for (d) double and (e) single pulse regimes.

causes a massive spiking in the electric field inside the fast rarefaction wave. This is normally associated with the heavy ion front, but it also occurs in simulations without any heavy ions. This spiking in the electric field leads to generation of a peak in the proton density. Once this is formed, the mechanism moves into a second stage where the peak in the proton density maintains a positive-going and negative-going spike in the electric field. The positive-going spike accelerates a bunch of protons to higher energy. This bunch then constitutes the peak that is seen in the energy spectrum.

In the PIC simulations that were carried out to test this concept, a scenario where two 40 fs pulses separated by a 100 fs delay was considered. The second pulse had a peak intensity of 4×10^{19} W cm^{-2}, and the peak intensity of the first pulse was varied between 7×10^{17} and 1×10^{19} W cm^{-2}. Fig. 6(a) shows the differences between single and double pulse simulations. In Fig. 6(b) we show the electric field and ion densities at representative times in both single and double pulse simulations. This illustrates the strong spiking in the electric field and the peaking in the proton density that is seen in the double pulse simulations.

As Fig. 6(a) shows, strong spectral peaks are generated. Future studies of this concept will need to improve upon this further and to develop an understanding of how the energy of the peak can be 'set' by controlling the laser parameters.

5. Summary and future challenges

We have shown that proton acceleration from thin foil targets irradiated by ultrashort high intensity laser pulses can be manipulated and controlled optically by the use of secondary laser pulses in a variety of schemes. The proton beam uniformity and flux have been shown to be enhanced by the creation of an optimum plasma density gradient using a separate low intensity laser pulse. It has been shown that the direction of proton beam acceleration can be steered using a controlled low temperature shock wave launched by a separate low intensity laser pulse. A scheme for controlling the spectral distribution of the accelerated proton beams through the use of an ultrashort prepulse has also been proposed and demonstrated in PIC simulations.

These techniques for optical control of the properties of laser-accelerated ion beams could be an important part of the strategy for developing applications which require dynamic control of ion pulses delivered at high repetition rate.

Acknowledgements

We acknowledge the expert support of the Vulcan laser team at the Central Laser Facility. This work was supported by the UK Engineering and Physical Sciences Research Council (EPSRC, grant number EP/E048668/1) and the Swedish Research Council.

References

[1] M. Borghesi, J. Fuchs, S.V. Bulanov, A.J. MacKinnon, P.K. Patel, M. Roth, Fusion Sci. Technol. 49 (2006) 412–439.
[2] S.C. Wilks, A.B. Langdon, T.E. Cowan, M. Roth, M. Singh, S. Hatchett, M.H. Key, D. Pennington, A. MacKinnon, R.A. Snavely, Phys. Plasmas 8 (2001) 542–549.
[3] S.V. Bulanov, T.Zh. Esirkepov, V.S. Khoroshkov, A.V. Kuznetsov, F. Pegoraro, Phys. Lett. A 299 (2002) 240–247.
[4] E. Fourkal, B. Shahine, M. Ding, J.S. Li, T. Tajima, C.-M. Ma, Med. Phys. 29 (2002) 2788–2798.
[5] V. Malka, S. Fritzler, E. Lefebvre, E. d'Humières, R. Ferrand, G. Grillon, C. Albaret, S. Meyroneinc, J.-P. Chambaret, A. Antonetti, D. Hulin, Med. Phys. 31 (2004) 1587–1592.
[6] S. Fritzler, V. Malka, G. Grillon, J.P. Rousseau, F. Burgy, E. Lefebvre, E. d'Humières, P. McKenna, K.W.D. Ledingham, Appl. Phys. Lett. 83 (2003) 3039–3041.
[7] K.W.D. Ledingham, P. McKenna, T. McCanny, S. Shimizu, J.M. Yang, L. Robson, J. Zweit, J.M. Gillies, J. Bailey, G.N. Chimon, R.J. Clarke, D. Neely, P.A. Norreys, J.L. Collier, R.P. Singhal, M.S. Wei, S.P.D. Mangles, P. Nilson, K. Krushelnick, M. Zepf, J. Phys. D 37 (2004) 2341–2345.
[8] P. McKenna, K.W.D. Ledingham, T. McCanny, R.P. Singhal, I. Spencer, M.I.K. Santala, F.N. Beg, K. Krushelnick, M. Tatarakis, M.S. Wei, E.L. Clark, R.J. Clarke, K.L. Lancaster, P.A. Norreys, K. Spohr, R. Chapman, M. Zepf, Phys. Rev. Lett. 91 (2003) 075006.
[9] P. McKenna, K.W.D. Ledingham, S. Shimizu, J.M. Yang, L. Robson, T. McCanny, J. Galy, J. Magill, R.J. Clarke, D. Neely, P.A. Norreys, R.P. Singhal, K. Krushelnick, M.S. Wei, Phys. Rev. Lett. 94 (2005) 084801.
[10] M. Schollmeier, S. Becker, M. Geissel, K.A. Flippo, A. Blažević, S.A. Gaillard, D.C. Gautier, F. Grüner, K. Harres, M. Kimmel, F. Nürnberg, P. Rambo, U. Schramm, J. Schreiber, J. Schütrumpf, J. Schwarz, N.A. Tahir, B. Atherton, D. Habs, B.M. Hegelich, M. Roth, Phys. Rev. Lett. 101 (2008) 055004.
[11] P. Antici, M. Fazi, A. Lombardi, M. Migliorati, L. Palumbo, P. Audebert, J. Fuchs, J. Appl. Phys. 104 (2008) 124901.
[12] M. Roth, T.E. Cowan, M.H. Key, S.P. Hatchett, C. Brown, W. Fountain, J. Johnson, D.M. Pennington, R.A. Snavely, S.C. Wilks, K. Yasuike, H. Ruhl, F. Pegoraro, S.V. Bulanov, E.M. Campbell, M.D. Perry, H. Powell, Phys. Rev. Lett. 86 (2001) 436–439.
[13] M. Temporal, J.J. Honrubia, S. Atzeni, Phys. Plasmas 9 (2002) 3098–3107.
[14] B.M. Hegelich, B.J. Albright, J. Cobble, K. Flippo, S. Letzring, M. Paffett, H. Ruhl, J. Schreiber, R.K. Schulze, J.C. Fernández, Nature 439 (2006) 441–444.
[15] H. Schwoerer, S. Pfotenhauer, O. Jäckel, K.-U. Amthor, B. Liesfeld, W. Ziegler, R. Sauerbrey, K.W.D. Ledingham, T. Esirkepov, Nature 439 (2006) 445–448.
[16] S. Ter-Avetisyan, M. Schnürer, P.V. Nickles, M. Kalashnikov, E. Risse, T. Sokollik, W. Sandner, A. Andreev, V. Tikhonchuk, Phys. Rev. Lett. 96 (2006) 145006.
[17] P.K. Patel, A.J. Mackinnon, M.H. Key, T.E. Cowan, M.E. Foord, M. Allen, D.F. Price, H. Ruhl, P.T. Springer, R. Stephens, Phys. Rev. Lett. 91 (2003) 125004.
[18] T. Toncian, M. Borghesi, J. Fuchs, E. d'Humières, P. Antici, P. Audebert, E. Brambrink, C.A. Cecchetti, A. Pipahl, L. Romagnani, O. Willi, Science 312 (2006) 410–413.
[19] M. Roth, A. Blažević, M. Geissel, T. Schlegel, T.E. Cowan, M. Allen, J.-C. Gauthier, P. Audebert, J. Fuchs, J. Meyer-ter-Vehn, M. Hegelich, S. Karsch, A. Pukhov, Phys. Rev. ST Accel. Beams 5 (2002) 061301.
[20] S. Kar, K. Markey, P.T. Simpson, C. Bellei, J.S. Green, S.R. Nagel, S. Kneip, D.C. Carroll, B. Dromey, L. Willingale, E.L. Clark, P. McKenna, Z. Najmudin, K. Krushelnick, P. Norreys, R.J. Clarke, D. Neely, M. Borghesi, M. Zepf, Phys. Rev. Lett. 100 (2008) 105004.
[21] S. Kahaly, S.K. Yadav, W.M. Wang, S. Sengupta, Z.M. Sheng, A. Das, P.K. Kaw, G.R. Kumar, Phys. Rev. Lett. 101 (2008) 145001.
[22] Y. Sentoku, V.Y. Bychenkov, K. Flippo, A. Maksimchuk, K. Mima, G. Mourou, Z.M. Sheng, D. Umstadter, Appl. Phys. B 74 (2002) 207–215.
[23] J.T. Seo, S.H. Yoo, S.J. Hahn, J. Phys. Soc. Jpn. 76 (2007) 114501.
[24] A. Maksimchuk, S. Gu, K. Flippo, D. Umstadter, V.Yu. Bychenkov, Phys. Rev. Lett. 84 (2000) 4108–4111.
[25] A. Yogo, H. Daido, A. Fukumi, Z. Li, K. Ogura, A. Sagisaka, A.S. Pirozhkov, S. Nakamura, Y. Iwashita, T. Shirai, A. Noda, Y. Oishi, T. Nayuki, T. Fujii, K. Nemoto, I.W. Choi, J.H. Sung, D.-K. Ko, J. Lee, M. Kaneda, A. Itoh, Phys. Plasmas 14 (2007) 043104.
[26] D.C. Carroll, P. McKenna, O. Lundh, F. Lindau, C.-G. Wahlström, S. Bandyopadhyay, D. Pepler, D. Neely, S. Kar, P.T. Simpson, K. Markey, M. Zepf, C. Bellei, R.G. Evans, R. Redaelli, D. Batani, M.H. Xu, Y.T. Li, Phys. Rev. E 76 (2007) 065401.
[27] P. McKenna, D.C. Carroll, O. Lundh, F. Nürnberg, K. Markey, S. Bandyopadhyay, D. Batani, R.G. Evans, R. Jafer, S. Kar, D. Neely, D. Pepler, M.N. Quinn, R. Redaelli, M. Roth, C.-G. Wahlström, X.H. Yuan, M. Zepf, Laser Part. Beams 26 (2008) 591–596.
[28] B. Dromey, S. Kar, M. Zepf, P. Foster, Rev. Sci. Instrum. 75 (2004) 645–649.
[29] G. Doumy, F. Quéré, O. Gobert, M. Perdrix, Ph. Martin, P. Audebert, J.C. Gauthier, J.-P. Geindre, T. Wittmann, Phys. Rev. E (2004) 026402.
[30] T.E. Cowan, J. Fuchs, H. Ruhl, A. Kemp, P. Audebert, M. Roth, R. Stephens, I. Barton, A. Blažević, E. Brambrink, J. Cobble, J. Fernández, J.-C. Gauthier, M. Geissel, M. Hegelich, J. Kaae, S. Karsch, G.P. Le Sage, S. Letzring, M. Manclossi, S. Meyroneinc, A. Newkirk, H. Pépin, N. Renard-LeGalloudec, Phys. Rev. Lett. 92 (2004) 204801.
[31] F. Nürnberg, M. Schollmeier, E. Brambrink, A. Blažević, D.C. Carroll, K. Flippo, D.C. Gautier, M. Gessel, K. Harres, B.M. Hegelich, O. Lundh, K. Markey, P. McKenna, D. Neely, J. Schreiber, M. Roth, Rev. Sci. Instrum. (2009), in press.
[32] G.J. Pert, J. Comput. Phys. 43 (1981) 111–163.
[33] O. Lundh, F. Lindau, A. Persson, C.-G. Wahlström, P. McKenna, D. Batani, Phys. Rev. E 76 (2007) 026404.
[34] R. Fonseca, L. Silva, F. Tsung, V. Decyk, W. Lu, C. Ren, W. Mori, S. Deng, S. Lee, T. Katsouleas, J. Adam, in: P.M.A. Sloot, et al. (Eds.), Lecture Notes in Computer Science, vol. 2331, Springer, Heidelberg, 2002, pp. 342–351.
[35] F. Lindau, O. Lundh, A. Persson, P. McKenna, K. Osvay, D. Batani, C.-G. Wahlström, Phys. Rev. Lett. 95 (2005) 175002.
[36] P. McKenna, F. Lindau, O. Lundh, D. Neely, A. Persson, C.-G. Wahlström, Philos. Trans. R. Soc. A 364 (2006) 711–723.

[37] O. Lundh, Y. Glinec, C. Homann, F. Lindau, A. Persson, C.-G. Wahlström, D.C. Carroll, P. McKenna, Appl. Phys. Lett. 92 (2008) 011504.
[38] A.P.L. Robinson, D. Neely, P. McKenna, R.G. Evans, Plasma Phys. Controlled Fusion 49 (2007) 373–384.
[39] N. Kumar, A. Pukhov, Phys. Plasmas 15 (2008) 053103.